A SIMPLE MODEL TO PREDICT CRITICAL RICOCHET ANGLE IN LONG-ROD PENETRATION

K. Daneshjou [*] **M. Shahravi** [**]

Department of Mechanical Engineering
Iran University of Science and Technology
Narmak, Tehran, Iran

ABSTRACT

The ricochet of eroding long rods, from steel targets, is investigated by a series of three-dimensional numerical simulations in explicit finite element code. These are compared with the predictions of our analytical model and experimental results for ricochet. This approach is different than the rigid body treatment by A. Tate. Also it uses a new penetration velocity equation to pre[illegible] critical ricochet angle. Critical ricochet angles were calculated for various impact velocities and st[illegible]f the target plates in these approaches. It was predicted that critical ricochet angle increases [illegible] impact velocities and that higher ricochet angles were expected if higher strength ta[illegible]mployed. New model's results show a better agreement with numerical results [illegible]han Tate and Rosenberg models.

Keywords : Critical ricochet angle, Long-rod, Analyti[illegible]

RETRACTED

1. INTRODUCTION

The phenomenon of ricochet is an i[illegible] eration in ballistics. While a large fra[illegible] generated ballistic data is gath[illegible] impact-conditions of normal i[illegible] mathematically probable r[illegible] listic impacts on the ba[illegible] level of impact obli[illegible] normal). At lo[illegible] listic effect o[illegible] creased l[illegible]rget. However, d[illegible]s of the rod and target[illegible] impact velocity, and yaw, [illegible]angle of obliquity at and beyon[illegible]cochets from the target surface.

Ricochet has been a[illegible]died phenomenon. An excellent review of work [illegible] the area is provided as a chapter in Goldsmith's review paper on projectile impact [1]. Much of the research in ricochet centers is on compact projectiles or on rigid projectiles. A much smaller fraction of the work is focused on medium- and long-rod ricochet, where a different phenomenology often manifests itself.

Radiographic evidence and hydrocode simulation of long-rod ricochet was presented by Jonas and Zukas [2] in 1978. With experimental radiography and corroborating hydrocode simulation, they demonstrate how the rod can form at the impact site (stationary with respect [illegible]d from a rigid target sur- [illegible] Jonas and Zukas was to [illegible]e modeling capability, no ana- [illegible]alysis was offered.

[illegible]3] developed an early model for the [illegible]s, in which the cylindrical rod (of square [illegible]n) responds as a rigid body away from the [illegible]tip. Tate's model allows the local erosive de-[illegible]ation of the rod in the immediate vicinity of the [illegible]pact. The asymmetric forces acting on this deforming rod tip are evaluated to ascertain their capacity to induce a rotation sufficient to bring about ricochet during the limited time before the rod tip becomes fully engaged in the target. While the model permits local deformation at the rod's tip, affecting the line of action of the interaction force, ricochet is judged to occur only if the remainder of the rod is adequately rotated, in a rigid fashion about its center of gravity, so as to produce a net linear velocity in the rod tip parallel to the target surface. Tate's approach produces an analytical expression for the target obliquity angle θ_{crit}, beyond which ricochet is predicted to occur. The expression for it is given as

Tate model:

$$\tan^3\beta > \frac{2}{3}\frac{\rho_P V^2}{Y_P}\left(\frac{L^2+D^2}{LD}\right)\left(\frac{V}{V-U}\right) \qquad (1)$$

where ρ_p is the rod's density, V is the striking velocity of the rod, Y_p is the yield strength of the rod, L and D are the rod's length and diameter, respectively, and U is the

[*] Professor [**] Ph.D. student

initial penetration velocity of the rod into the target. Note that the need for the penetration velocity U as input to the model requires an auxiliary calculation from a ballistic penetration model, such that U, in addition to the rod variables already listed, becomes a function of the target resistance and the target density.

One of the drawbacks of the Tate ricochet model is its failure to predict ricochet for the rigid-rod (*i.e.*, $U = V$) scenario, because of the method used to calculate the line of action of the interaction force. Further, because of the model's requirement to ricochet by way of rigid-rod rotation, ricochet becomes increasingly improbable as the rod length is increased.

Jonas and Zukas [2], Senf *et al*. [4] showed in 1981 how the ricocheting rod can form a deformable shape at the impact site to deflect the rod from a rigid target surface. Such observations provided additional evidence that, even in the absence of erosion, a rigid rod assumption does not necessarily hold during the ricochet process. Like Jonas and Zukas, the intention of Senf *et al*. was to demonstrate hydrocode modeling capability, and so no additional analysis was offered.

Reid *et al*. [5] began to address, with analysis, the notion of the plastic hinge, traveling down the rod's length, but stationary with respect to the target surface. In their analysis, they simplified the problem to consider only the transverse bending forces, and were able t[illegible] analogize the problem to one of a transverse impac[illegible] the free end of a cantilever beam.

Johnson *et al*. [6] studied ricochet int[illegible] plasticine (modeling clay) rods and t[illegible] upon predictions from Tate's ricoche[illegible] son *et al*. limited their testing [illegible] above 75°. Photographic rec[illegible] rod behavior similar to that [illegible] [2], Senf *et al*. [4].

By 1983, several [illegible] the ricochet prob[illegible] results. The [illegible] the impact[illegible]gets, with new an[illegible]n. The impact veloci[illegible] obliquities were restricted t[illegible]ir work seems to focus more on t[illegible]ct problem of rod buckling as the prin[illegible] deformation, rather than bending associated [illegible]ochet deflection.

Rosenberg *et al*. [8] re[illegible]ited the ricochet problem in 1989. They acknowledge adapting many of Tate's [3] original premises, concerning the origins of the asymmetric force that acts upon the eroding tip of the impinging rod. However, the key point of departure for Rosenberg *et al*. is in assuming that the interaction force acts only upon the mass actively engaging the target, and not upon the wholly remaining rigid rod as Tate assumed. Thus, in the Rosenberg model, the interaction force acts to linearly deflect rod-tip material in the transverse direction, rather than acting to apply a rotational moment upon the rigid rod, as in the Tate ricochet model.

Rosenberg model

$$tg^2\beta > \frac{\rho_P V^2}{R_T}\left(\frac{V+U}{V-U}\right) \tag{2}$$

where R_t is the target resistance. Like Tate's model, the Rosenberg model's need for the penetration velocity U as input demands a further calculation that requires, in addition to those variables listed, knowledge of the rod strength Y_p and the target density. The model was shown to have good prediction ability for $L/D = 10$ tungsten (WA) rods launched against rolled homogeneous armor targets at striking velocities between 600 and 1400m/s and target obliquities between 55° and 75°.

The interaction methodology of Rosenberg *et al*. however, calculates the force interaction based upon a virgin, long-rod striking an erodible (but as yet undeformed) target. Thus it would seem that the methodology should only [illegible] prediction as to what happens to the initial [illegible]aterial against the target. Once the initia[illegible]lected, for example, the geometric "[illegible]e remaining rod and gouged [illegible] harmony with the mod[illegible]n indicates that th[illegible]bserved cases [illegible]via ricochet fol[illegible]establishing penetra[illegible]m which it is derived, [illegible]own under conditions in [illegible]gid (*i.e.*, when $U = V$), because [illegible]n the interaction force's line of [illegible]

[illegible] studies of the ricochet phenomenon fo[illegible]ical projectiles [9], rigid projectiles [10], [illegible]onal methods [11], or else touch on ricochet [illegible]eripherally as part of a larger examination [12,13]. [illegible]ne of these studies offer additional analytical modeling insight into the phenomenology of medium- and long-rod ricochet.

2. MODEL CONSTRUCT

We adopt Rosenberg's arguments concerning the source of the asymmetric force acting on the tip of the long rod as it engages the oblique target. This interaction is shown in Fig. 1. which is taken from Rosenberg's work [8].

As in [8] we assume that the tip of the rod is eroding according to Rosenberg's theory [8]. and that the cross section of the rod is square, in order to simplify the analysis. Thus the same relations can be derived for the angle ψ (see Fig. 1) and the length (S) of the eroding tip [8].

$$\frac{S\cdot\sin\psi}{x} = tg\psi \tag{3}$$

$$V - U = \frac{S\cdot\sin\psi}{t}$$

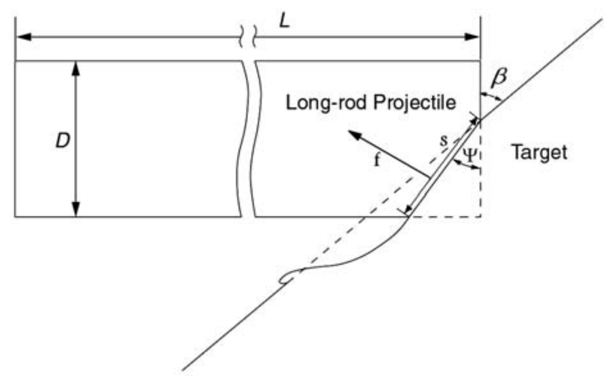

Fig. 1 The asymmetric interaction between rod and target some time after impact (from [8])

The force (f) which acts on the eroding surface is responsible for the bending of the rod and for its ricochet. Rosenberg assumed that the magnitude of this force depends on the pressure which the target exerts on the projectile. Thus, used the strength parameter R_T for the target. and wrote for the force f:

$$f = R_T \cdot S \cdot D \tag{4}$$

where $S{\cdot}D$ is the area of the eroding surface of the rod. Only the vertical component of f is of interest (f sinψ) and the time is needed for the whole tip of the rod [illegible] reach the target is $tm = D\, tg\beta / V$. Thus, the [illegible] impulse imparted by the asymmetrical force [illegible] tip of the rod is:

$$I = \int_0^{t_m} f \cdot \sin\psi \cdot dt = \frac{R_T D^3 (V - [illegible]}{2V [illegible]}$$

The relevant mass, on [illegible] is smaller than the [illegible] amount of the [illegible]

$m2 = \frac{\rho_P D^2 \cdot ([illegible]}{}$ [illegible] ass

of the rod ti[illegible]

$$m = m_1 - m [illegible] \tag{6}$$

Using momentum co[illegible]on we get from Eqs. (3) and (4):

$$\rho_P D^3 tg\beta \cdot \frac{V+U}{2V} V_T = \frac{R_T D^3}{2} \cdot \frac{V-U}{V^2} \cdot tg^2\beta \tag{7}$$

Where V_T is the vertical velocity imparted by the asymmetrical force (f) to the tip of the rod (Fig 2). Form Eq. (7) we get:

$$V_T = \frac{R_T}{\rho_P V^2}\left(\frac{V-U}{V+U}\right) V \cdot tg\beta \tag{8}$$

In spite of Rosenberg method we use a new approach for penetration velocity as below:

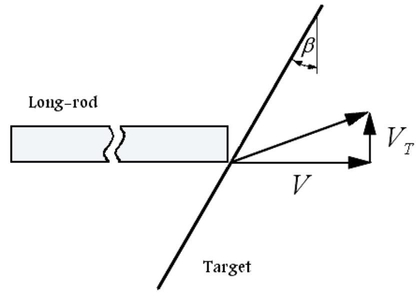

Fig. 2 The velocity vectors of the rod

First step considered here is the development of a relationship between erosion rate, $\dot{l}$, and the instantaneous velocity of the un-deformed portion of the rod v. For a cylindrical penetrator of length L and diameter D, the greater the instantaneous velocity of the rod, the higher the erosion rat[illegible] Therefore, it seems appropriate to assume that e[illegible], $\dot{l}$, is proportional to this velocity. Empl[illegible]ept, the following relation is assum[illegible]8]

$$[illegible] \tag{9}$$

wh[illegible]y of material [illegible] erosion rate and [illegible]esent as $\dot{l}/\nu$. As [illegible]ent to material proper[illegible] It is not dependent to pro[illegible], this is a useful parameter to [illegible]g-rod penetration phenomena. [illegible]anging the projectile geometry, the [illegible]n additional experimental set up to obtain [illegible] remove. The other reason may be the fact [illegible] parameter α is simplified in hypervelocity re[illegible]

RETRACTED

Using the above assumption along with kinematic relationships about long-rod penetration:

$$\dot{l} = (u - v) \tag{10}$$

results in:

$$u = v\,(1 - \alpha) \tag{11}$$

Equation (11) is a relation between u and v if the dependency of α on material properties is established.

At this point it is appropriate to attempt to determine what type of a relationship should exist between u and v. The objective is to develop a mathematical relationship based on the physics of the problem as follows:

1. At hyper velocities the relationship between u and v should be independent of the strength properties of the target and penetrator. (Classical jet penetration formula $Z = L\sqrt{\frac{\rho_P}{\rho_T}}$; Where ρ_p and ρ_T are projectile and target density that shown in Figs. 3 and 4).
2. At low velocities the relationship between u and v should depend on the strength properties of the impacting materials.

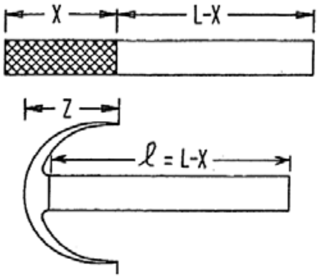

Fig. 3 Schematic of rod in penetration process (a) plastic portion X and undeformed portion L-X (b) penetration into target to a depth Z

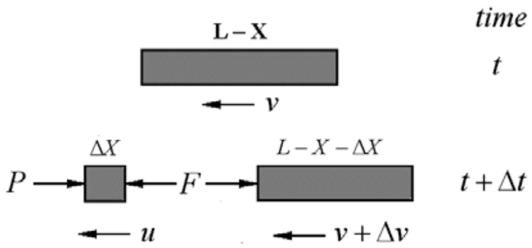

Fig. 4 Schematic diagram of mass transfer from the undeformed to the plastic portion of the rod

3. Since $l = -(v-u)$, the higher the difference between [illegible] v and u, the higher the erosion rate. For a gi[illegible] material, higher erosion rate corresponds t[illegible] impact velocity. This translates into the [illegible] higher values of impact velocity v, [illegible] between v and u will be higher. [illegible] at low impact velocity, the ero[illegible] to be low and the differen[illegible] creases.
4. In an impact situati[illegible] the ultimate yield [illegible] tor. That is, [illegible] of the targ[illegible] tance to [illegible]en-sile stre[illegible] condi-tions unc[illegible] strength penetrator t[illegible] a rigid body and consequen[illegible]to the target.

Considering the a[illegible]es, at hypervelocity the relation between u a[illegible]s the following form:

$$u = \frac{v}{1+\sqrt{\left(\frac{\rho_T}{\rho_P}\right)}} \tag{12}$$

This relationship is obtained if fluid behavior is assumed for the colliding materials (negligible structural resistive forces) and the momentum equation is applied as follows:

$$\rho_P (v-u)^2 = \rho_T u^2 \tag{13}$$

Solving Eq. (13) for u will result in Eq. (12). Now, at hypervelocity there are two relationships between u and v, Eq. (12), and relation assumed previously, Eq. (11). Comparing these two equations we obtain:

$$v(1-\alpha) = \frac{v}{1+\sqrt{\left(\frac{\rho_T}{\rho_P}\right)}} \tag{14}$$

From which an expression for α can be obtained as

$$\alpha = \frac{\lambda}{\lambda+1} \tag{15}$$

where λ is the square root of the ratio of the density of the target to the density of the penetrator

$$\lambda = \sqrt{\left(\frac{\rho_T}{\rho_P}\right)} \tag{16}$$

Equation (15) is valid a[illegible] hypervelocity only and does not apply at low im[illegible]elocity. This term can be thought of as a li[illegible]t velocity becomes very high,

[illegible] (17)

[illegible]low velocity, [illegible]ole and the rela-[illegible] on these parameters. [illegible]r of possibilities to ar-[illegible] expression between these [illegible]ing exponential relation was [illegible]thermore, the results of many test [illegible]d in relation 18 as an exponential [illegible] help of curve fitting method:

$$\alpha = \frac{\lambda}{1+\lambda}\left[1-\left(\frac{\gamma}{1+\gamma}\right)e^{-v\left(\frac{\rho_P}{Y_P}\right)^{1/2}}\right] \tag{18}$$

where γ is the ratio of the target ultimate strength to that of the penetrator

$$\gamma = \left(\frac{Y_T}{Y_P}\right) \tag{19}$$

The properties of this exponential expression are as follows:

1. At hypervelocity the exponential part of the expression for α goes to zero and the relation between u and v becomes independent of the strength properties of the materials and reduces to the classical density law

$$u = \left[1-\frac{\lambda}{1+\lambda}\right] v \tag{20}$$

2. At lower velocity the effect of the strength terms become pronounced as v decreases. The value of α increases as the difference between v and u decreases corresponding to the fact that at low velocity the erosion rate becomes smaller. The relationship between u and v in this situation is

RETRACTED

$$u = v\left[1-\frac{\lambda}{1+\lambda}\left(1-\left(\frac{\gamma}{1+\gamma}\right)e^{-v\left(\frac{\rho_P}{Y_P}\right)^{1/2}}\right)\right] \tag{21}$$

Equation (21) corresponds to all the guidelines indicated previously and is considered to be a valid expression relating u and v. This equation also indicates that u is always less than or equal to v as expected and the internal consistency of the problem is sustained.

From Eqs. (8) and (21) we get:

$$V_T = \frac{R_T}{\rho_P V^2}\left[\frac{\frac{\lambda}{1+\lambda}\left(1-\left(\frac{\gamma}{1+\gamma}\right)e^{-v\left(\frac{\rho_P}{Y_P}\right)^{1/2}}\right)}{2V-\frac{\lambda}{1+\lambda}\left(1-\left(\frac{\gamma}{1+\gamma}\right)e^{-v\left(\frac{\rho_P}{Y_P}\right)^{1/2}}\right)}\right] V\cdot tg\beta \tag{22}$$

Figure 2 shows the two velocity vectors of the rod and one can easily show that ricochet occurs if

$$tg\beta > \frac{V}{V_T}\ .$$

Then we have:

$$tg^2\beta > \frac{\rho_P V^2}{R_T}\left[\frac{2-\frac{\lambda}{1+\lambda}\left(1-\left(\frac{\gamma}{1+\gamma}\right)e^{-v\left(\frac{\rho_P}{Y_P}\right)^{1/2}}\right)}{\frac{\lambda}{1+\lambda}\left(1-\left(\frac{\gamma}{1+\gamma}\right)e^{-v\left(\frac{\rho_P}{Y_P}\right)^{1/2}}\right)}\right]$$

This relation shows a be[illegible] because it has additiona[illegible] model.

3[illegible]

A full [illegible] element analysis wit[illegible] ed on the principle of virt[illegible] fference time integration scheme [illegible] d out to investigate the ricochet p[illegible] ce theoretical and mathematical foundatio[illegible] e explicit finite element analysis are well establi[illegible] d [14,15] and are widely adopted to solve the problem of high-strain-rate deformations [16], the lengthy derivation of the equations for the numerical analysis is not repeated here. A general-purpose explicit finite element analysis code was used for the numerical calculations.

Figure 5 shows a typical finite element model used in the numerical analysis. The model consists of a rectangular oblique target plate and a cylindrically shaped projectile with blunt nose shape that is initially located 1mm away from the target. Only half of the whole geometry was modeled due to the inherent symmetry of the model along the x-direction of the coordinate as shown in Fig. 5. The length and diameter of the projectiles chosen for the numerical analysis were 75 and 7mm, respectively, giving an L/D ratio of 10.7. Impact velocities of the projectiles were varied from 1000 to 2000m/s with an increment of 250m/s. Target plates modeled are l50mm long, 40mm wide and 6.25mm thick. Obliquity of the plates was varied from 3° to 25° with intervals of 1°. Typical eight-node linear brick elements with reduced integration were used for meshing as shown in Fig. 3. Material properties were applied to the model by assigning appropriate material properties to the pre-defined projectile and target element sets, *i.e.*, properties of WHA to the projectile element set and properties of the two types of high hardness steel, namely, RHA class 4 [17] and S-7 tool steel [18], to the target element set.

In order to model a high-strain-rate mechanical response of the projectile and the target materials, a commonly used constitutive equation, the Johnson-Cook Eq. [18], was used as it is known to describe high-velocity mechanical response[illegible] umber of metals fairly well [19]. This has th[illegible]

$$\sigma = (\sigma \ldots \left[\ldots\left(\frac{T-T_r}{\ldots-T_r}\right)^m\right] \tag{24}$$

[illegible] p the effective [illegible] e, $\dot{\varepsilon}_0$ the reference [illegible] he room temperature, [illegible] d B, C, m and n are mate[illegible] materials used in this study, [illegible] determined from separate ex[illegible] A and WHA) or taken from Johnson [illegible] S-7 tool steel) [18] and are shown in Ta[illegible] her with the basic physical properties re[illegible] or the calculations.

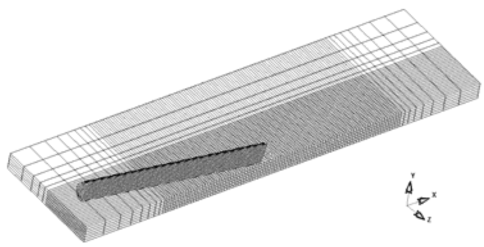

Fig. 5 Typical finite element mesh coordinate system used for the numerical study in this work

Table 1 Material properties and constants for the Johnson-Cook model applied to the numerical model

	WHA	RHA	S-7
Shear modulus (GPa)	152.02	76.96	79.96
$\rho(\mathrm{kgm^{-3}})$	17000	7840	7750
Specific heat ($\mathrm{Jkg^{-1}K^{-1}}$)	134	477	477
T_m (K)	1723	1809	1763
σ_0 (MPa)	1410	1160	1539
B (MPa)	223.3	415.9	477
n	0.11	0.28	0.18
C	0.022	0.012	0.012
m	1.0	1.0	1.0

The interaction between the projectile and the plate was simulated by a Lagrangian-Lagrangian contact algorithm based on a slave-grid/master segment concept. This algorithm checks eventual penetration of slave-grids through master segments and applies constant forces to push them back. Erosion of the projectile and the target was simulated through a so-called adaptive contact algorithm [20], which automatically updates contact definition between the interacting deformable bodies upon elimination of the elements when pre-set level of plastic strains, determined by a separate depth of penetration (DOP) calibration, are reached.

4. EXPERIMENTAL

Experiments were carried out to verify the numerical results. These results were used from last papers. The experimental set-up shown in Fig. 6 was used in last papers consists of three witness blocks (38mm thick RHA class 4), an oblique target plate (6.25mm thick RHA class 4), a velocity-measuring device and a solid propellant gun. WHA projectiles with L/D ratios of 10.7 (L = 75 and D = 7mm) were impacted at velocities of about 1000 and 1500ms^{-1}. The velocities of the projectiles were controlled by adjusting the amount of solid propellant charge. The relations between th[illegible] amount of the charge and the projectile velocities [illegible] calibrated in a preparatory experiment.

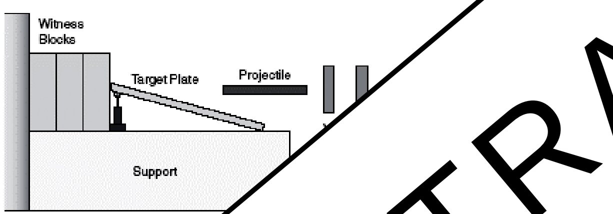

Fig. 6 Schemat[illegible] up fo[illegible] lo[illegible] per- for[illegible]

5. RESU[illegible]USSION

5.1 Post-Impact Beha[illegible] the Projectile and the Target Plate

Numerical results are graphically shown in Figs. 7 ~ 9 in terms of the mesh deformation with the lapse of time to analyze the behavior of the WHA projectile and the RHA target with thickness comparable to the projectile diameter during the oblique impact. When the projectile impact velocity is 1000ms^{-1} and the target oblique angle is 10°, as in the case shown in Figs. 7(a) ~ 7(h), the projectile initially bends on impact (Fig. 7(a)). Subsequently, a plastic hinge is formed which remains at the initial point of impact with respect to a fixed coordinate system (Eulerian) resulting in its relative backward motion along the x-direction of the coordinate system (Fig. 5) as the projectile progresses forward (Figs. 7(b) ~ 7(d)). In the case being considered (θ = 10°), where the oblique angle is lower than the critical ricochet angle, the target does not deform much and no significant erosion of the impacted surface is noticed whilst the front end (denoted as head hereinafter) of the projectile lifts from the target surface after sliding some distance and eventually the projectile bounces away (Figs. 7(e) ~ 7(h)). Such behavior is yielded due to the asymmetric reaction force exerted from the contact area to the projectile, which is reportedly proportional to the area of the contact, target strength and oblique angle [8].

When the oblique angle of the target plate is increased to 12° whilst keeping the impact velocity the same, the projectile shows somewhat different behavior. As shown in Figs. 8(a) ~ 8(d), it initially pushes the impacted area of the target inward following impact since the target plate is a[illegible]owed.

Whilst the head of [illegible]jectile tends to bounce back from the target d[illegible]ction force exerted from the contact ar[illegible] of the impact, its trailing portion[illegible]er) tends to penetrate into th[illegible]l trajectory of the initi[illegible], the front part a[illegible]nd slid on the [illegible]ear part behind it [illegible] forming a stretched [illegible]pact crater in the target [illegible]ed, the relatively thin de[illegible]gnificant role in yielding such [illegible]ritical oblique angle, the tail also [illegible] later time step before it completely [illegible]rget achieving critical ricochet (Fig. 8(h)). [illegible] the elongation of the projectile becomes so [illegible]t it results in the fragmentation of the projectile. [illegible] the case where the oblique angle is further in[illegible]eased to 14° beyond the critical angle, as can be seen in Figs. 9(a) ~ 9(c), the initial behavior of the projectile and the target is similar to the case of critical ricochet shown in Figs. 8(a) ~ 8(d).

However, unlike in the previous case, the tail part further progresses to penetrate into the target downward by eroding it (Figs. 9(e) and 9(f)), resulting in the fragmentation of the projectile due to extreme elongation as well as complete penetration (perforation) of the target as shown in Figs. 9(g) and 9(h).

Understanding the physical nature of the above behavior of the projectile and the target can be supplemented by analyzing the changes in the projectile velocities after impact, as has also been performed for normal penetration in the literature [21]. For this purpose, post-impact changes in the horizontal (along the x-direction) and vertical (along the y-direction) velocities of head and tail of the projectile have been monitored during the numerical calculations and the results are plotted in Figs. 10 to 15. Before impact, the head and the tail move at the same initial velocity of 1000ms^{-1} and there is no vertical velocity term. For the case with relatively low oblique angle, *e.g.*, θ = 10°, as shown in Figs. 10 and 11, the horizontal velocities of

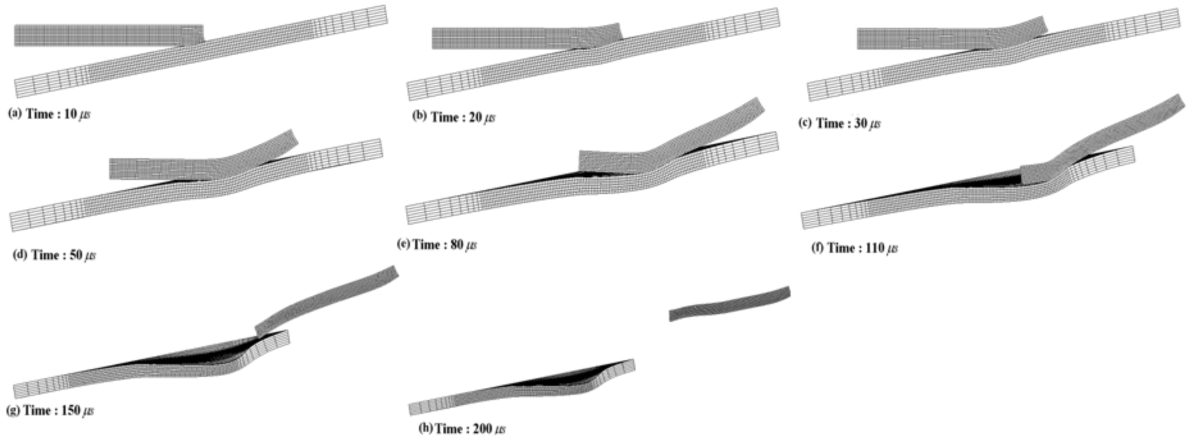

Fig. 7 Numerical results showing the behavior of the WHA projectile and the RHA target when the oblique angle is 10° and the impact velocity is 1000m/s

RETRACTED

Fig. 8 Numerical re… rojectile and the RHA target when the oblique angle is 12° and th…

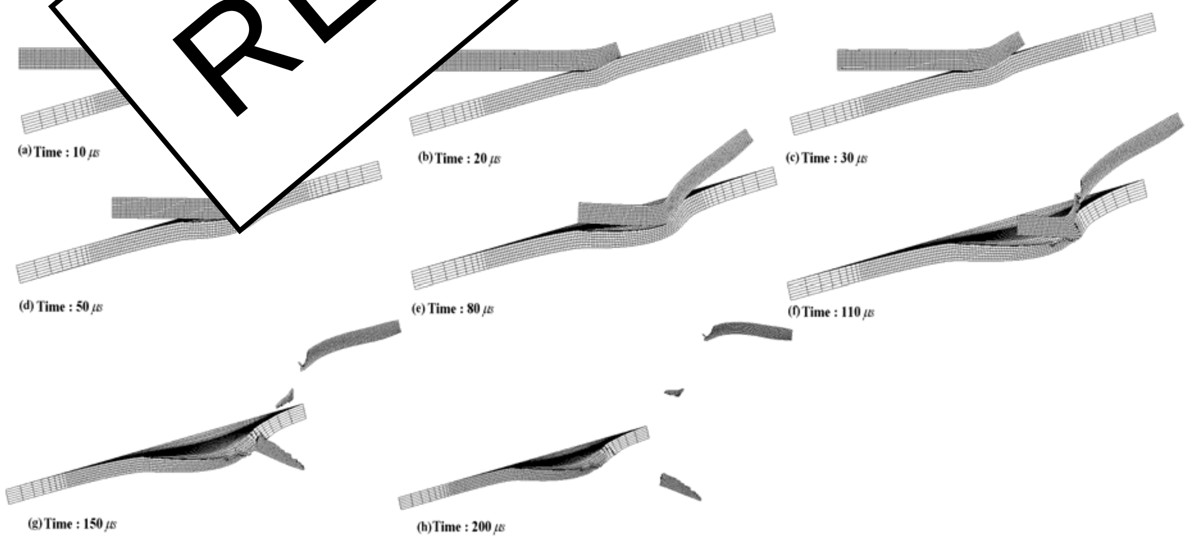

Fig. 9 Numerical results showing the behavior of the WHA projectile and the RHA target when the oblique angle is 14° and the impact velocity is 1000m/s

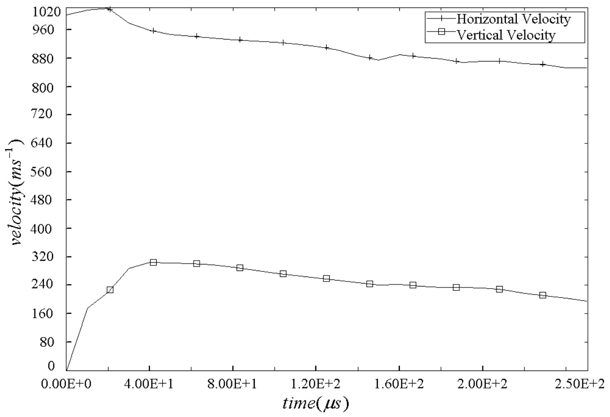

Fig. 10 Projectile head horizontal and vertical velocity ($\theta = 10°$)

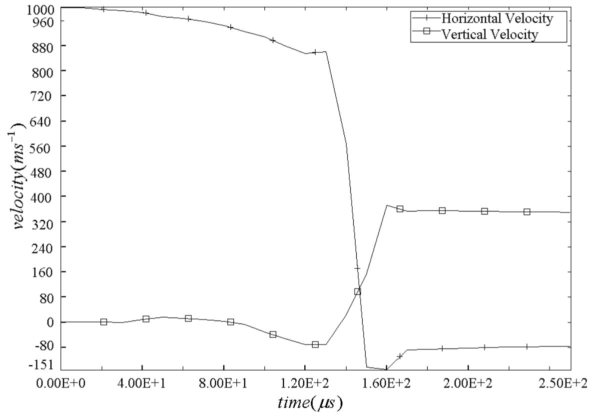

Fig. 13 Projectile tail horizontal and vertical velocity ($\theta = 12°$)

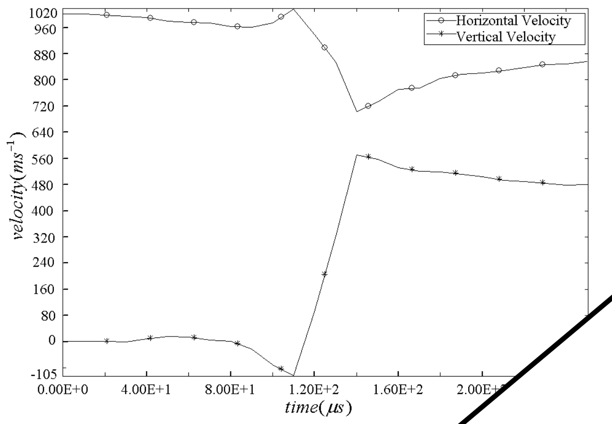

Fig. 11 Projectile tail horizontal and vertical velocity ($\theta = 10°$)

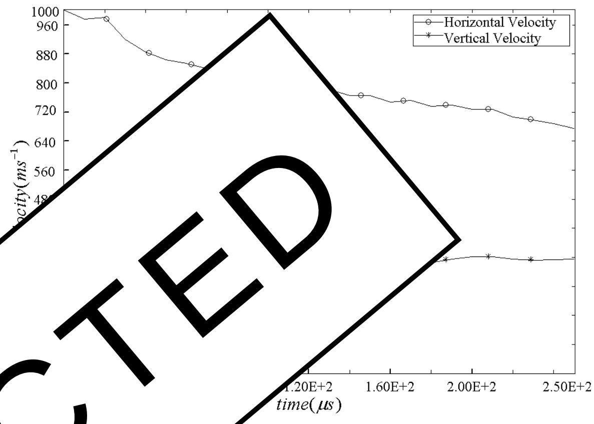

Fig. 14 Projectile head horizontal and vertical velocity

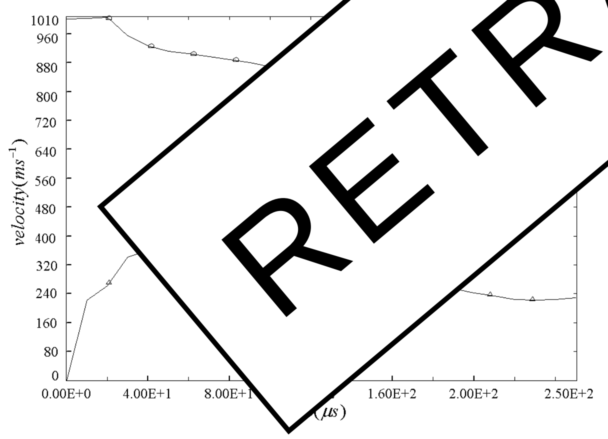

Fig. 12 Projectile head horizontal and vertical velocity ($\theta = 12°$)

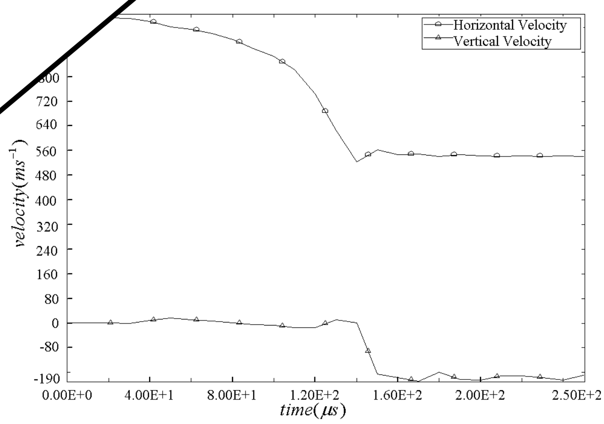

Fig. 15 Projectile tail horizontal and vertical velocity ($\theta = 14°$)

the head and the tail of the projectile after impact are kept almost identical, implying no significant axial strain, which prevents the projectile segmentation. It can also be seen that the horizontal velocities did not decrease noticeably. From this, it is inferred that the projectile does not encounter any significant resistance to its motion along the flight trajectory and that the impact interaction of the projectile with the target does not cause any large-scale deformation of the target.

Whilst there were only slight changes in the horizontal velocities, vertical velocities of the head and the tail undergo noticeable changes during the impact process. As can be seen in Fig. 10, the vertical velocity of the head initially increases to about 300ms^{-1} and remains almost the same thereafter, which would be associated with sliding on the target surface and subsequent takeoff of the head shown in Figs. 7(a) ~ 7(h). On the other hand, the vertical velocity of the tail is almost 0 until about 80μs and then increases to about 550ms^{-1} at 140μs. This indicates that the impact of the head on the target does not cause any yawing force in the rear part of the projectile which is beyond the plastic hinge mentioned above. Near-constant vertical tail velocity of 460ms^{-1} after about 160μs would indicate the takeoff of the tail as shown in Figs. 7(f) and 7(h).

However, where critical ricochet was achieved (θ = 12° for the case considered herein), as shown in Fig. 12, the decrease in the horizontal velocity of the head with respect to time is more pronounced than in the previous case, indicating that the progress of the head is hindered more. In particular, as shown in Fig. 13, the horizontal velocity of the tail decreases to almost 0 from about 140μs, producing a velocity difference between the head and the tail of about 750ms^{-1}. Such a large velocity difference may cause large-scale deformation and therefore it would explain the stretching of the projectile shown in Fig. 8(g) followed by the segmentation of the projectile shown in Fig. 8(h). At the same time, a sudden drop in the horizontal velocity of the tail between 100 and 150μs is believed to be related to the target cratering shown in Figs. 8(f) and 8(g), which could exert a high resistance to the advance of the tail. When critical ricochet is achieved, even though the impact crater is formed on the target, this does not lead to target perforation. This can be explained from th changes in the vertical velocities of the head and th shown in Figs. 12 and 13, where it can be seen head and the tail sequentially acquire positi velocity components. They begin to tak target plate at about 0 and 150μs, res ing no further penetration of the ta

A similar trend is obtained angle is further increased, e 14 and 15 whilst two a First, the horizontal creased to abou nearly consta

tion is no longer hindered by the target thereafter, probably due to the earlier segmentation of the projectile. In the previous case shown in Fig. 12, the head portion was connected to the tail portion through the elongated portion until the later time step so that the tail, still staying in the impact crater in the target, delayed the propagation of the head, which is represented as continuously decreasing velocity. Second, the behavior of the tail after segmentation is completely different: the vertical velocity of the tail decreases to a negative value of about –180ms^{-1} from about 150ms^{-1}, which is then maintained almost constant after about 180μs. This indicates that the fragmented tail is heading downward, which would be responsible for the perforation of the target shown in Fig. 9(h).

The ricochet behavior illustrated in Figs. 7(a) to 9(h) are also supported by the experimentation carried out herein. Figure 16 sho the shape of the target plate and the witness blo the ricochet experiments. In this figure, the ape of the plate is apparent with an ical perforation hole. Occurrence ed by observing deformed target plate and pen When a projecti blique angles be seen in Figs. s resulted in a long formed by erosion, and on the witness block. At higher than the critical value, broke into two parts, resulting in henomenology in the target plate and k shown in Figs. 16(b) and 16(d): there nt groove (crater) followed by a single per hole in the target resulting from initial erosion subsequent penetration whilst two penetration es are noticeable in the witness block, one over and the other below the white line in Figs. 16(b) and 16(d) where the edge of the target was located.

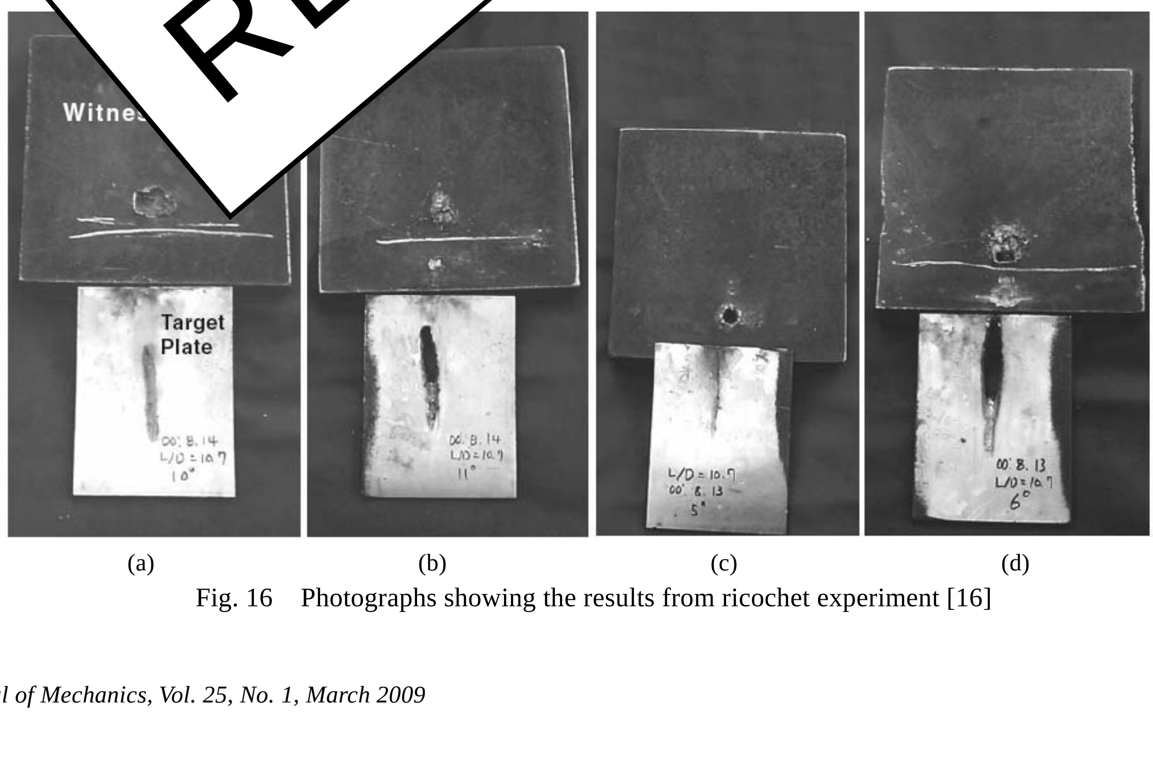

(a) (b) (c) (d)

Fig. 16 Photographs showing the results from ricochet experiment [16]

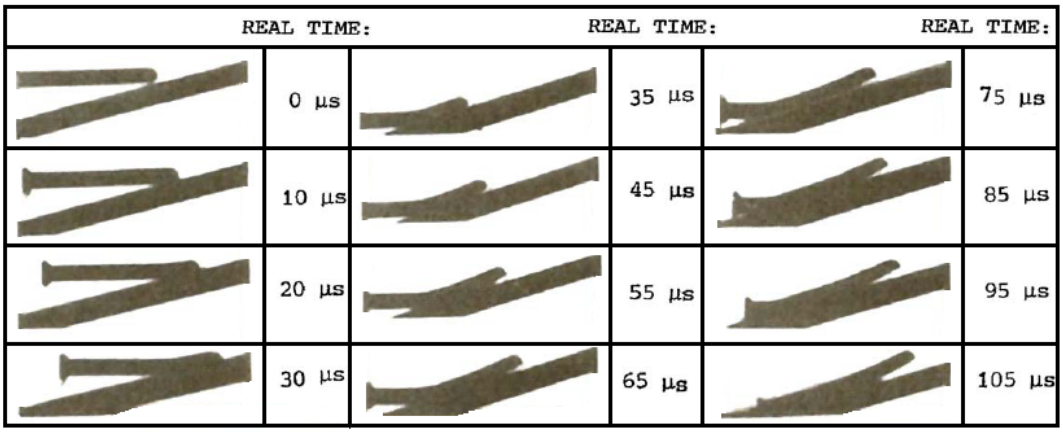

Fig. 17 Spark cinematography of a ricocheting rod projectile [4]

The post-impact behavior of the deformable projectile and the deformable target with finite thickness described so far in general agrees qualitatively with what has been observed and predicted in the previous works in which ricochet occurred at un-deformable (and sometimes rigid) target surfaces. However, as apparent in Figs. 7(a) to 9(h), the inward deformation of the target plate due to the finite thickness comparable to the projectile diameter is shown to assist the segmentation of the projectile, followed by the perforation of the target plate by the broken rear part of the projectile. S[illegible] phenomena could be responsible for the diffic[illegible] obtaining ricochet from relatively thin plates.

Senf *et al.* [4] showed how the ricoch[illegible] form a plastic hinge at the impact site [illegible] from a rigid target surface. These [illegible] 17) are similar the FEM solution [illegible] 7(a) to 9(h). But in FEM so[illegible] rigid and it deflected more [illegible]

5.2 Critical Ric[illegible]

In accorda[illegible] tioned in th[illegible] rico- chet angles [illegible] merical results graphi[illegible] last section and were p[illegible] pact velocities in Fig. 18 for the R[illegible] he ricochet angle curves shown in Fig[illegible] btained from curve-fitting the numerical re[illegible] a first-order exponential decay function. The fit[illegible] equations, their parameter values, and the statistical analysis of the fitted results are also reported in the figure. The numerical results are confirmed with experimental results as shown in Fig. 18. In Fig. 18, the hollow circle markers indicate perforation of the RHA target plate by the long-rod projectile whilst the solid star markers indicate critical ricochet of the projectile. It can be seen that there is good agreement between the two.

The new developed model results on the critical ricochet angles are also compared with experimental, numerical results and existing two-dimensional analytical models developed by Tate [3] and Rosenberg *et al.* [8], independently. The critical ricochet angles based on these models have been calculated for a WHA long- rod projectile and a RHA [illegible] as functions of impact velocities in Fig. 19[illegible]wn are the corresponding numerical resu[illegible]en in the figure that the Tate model [illegible]cal ricochet angle for impact v[illegible]$^{-1}$ and vice versa for lowe[illegible] the Tate curve is di[illegible]fference in the [illegible]y of interest ei[illegible]ms^{-1}. On the other [illegible]osenberg *et al.* shows a [illegible] results, though the former [illegible] ricochet angles at all impact [illegible]

[illegible]sults show a better agreement with [illegible]s. As shown Fig. 19, the difference [illegible] analytical model prediction result and [illegible] model result decrease up to 25%. The re[illegible] presented in this model, shifts to the experimental [illegible]lts, because:

1. This method was more detailed parameters to calculate the penetration velocity such as projectile density in comparing with Rosenberg analytical method.

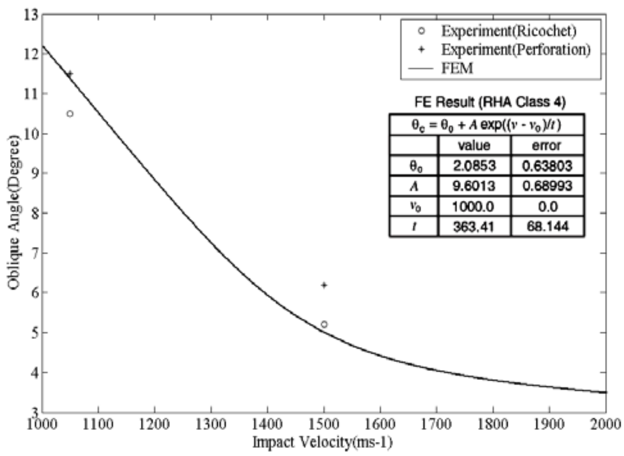

Fig. 18 Comparison of the numerically predicted critical ricochet angles for various velocities with the experimental results

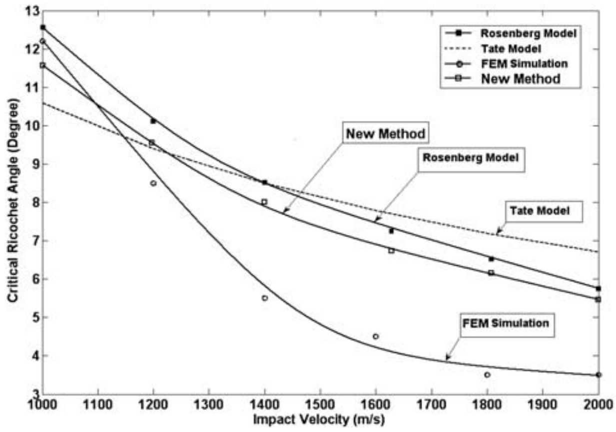

Fig. 19 Comparison of the numerically determined critical ricochet angles for various velocities with those predicted from two dimensional analytic models of Tate [6] and Rosenberg *et al*. [7] and new method

2. This method uses parameter α in calculating the critical ricochet angle, where α is based on the experimented results. Therefore the results might be were accurate.

Therefore new analytical model can be used as a practically useful guideline to estimate ricochet angles rather than existing two-dimensional analytical mod[els] developed by Tate [3] and Rosenberg *et al.* [8].

About effects of the target strength we hav[e]

Whilst the RHA has been widely use[d] armor material over decades, in som[e] material such as high hardness a[...] been adopted, though its use [...] toughness. To investiga[te] strength on the ricochet [...] in the Johnson-Cook [...] static yield streng[th] [...] duced by Thys[...] erature [17] [...] The ricochet an[gles] [...] plotted as a function [...] It can be seen that a high[...] [...]d for a given impact velocity i[f] [...] increased.

RETRACTED

5.3 Summary and Co[nclusio]ns

Ricochet of a WHA long-rod projectile impacting on oblique, steel target plates with finite thickness was investigated numerically using a full, three-dimensional, explicit finite element method with the predictions of our analytical model. Effects of the impact velocities of the projectiles and the hardness of the plates on the critical ricochet angle were considered.

It was predicted in the numerical analysis that the projectile and the target behave in three different ways depending on the oblique angle of the target. For a relatively low oblique angle, the impacted projectile bent and slid on the target surface to bounce away with very little velocity drop whilst no significant deformation of

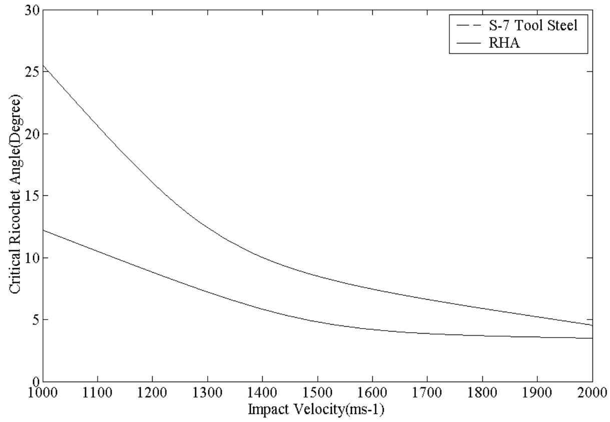

Fig. 20 Effect of target strength on the critical ricochet angles

the target was predicted. With increasing oblique angle, the projectile initiall[y] [...]n impact but the target deformed substantia[lly] [...]e tail portion of the target behind the pl[...] [...]sulted in the projectile stretching [...] [...]ail, which pulled the tail out [...] [...]l ricochet. Segme[...] [...]ed. When the [...] [...]jectile impact [...] [...]ayed the role of [...] [...]le through the target [...] case the projectile broke [...] Such behavior of the pro[...] [...]es predicted in this numerical [...] experimental observations of the [...] the target plates and the penetration [...]ness blocks. The post-impact behavior [...]able projectile and deformable target with [...]ckness in this work in general agreed qualita[tively] with previous work based on un-deformable (and [ri]gid) target surfaces. However, the deformable target assisted the breakage of the projectile followed by the perforation of the plate by the broken rear part of the projectile.

Critical ricochet angles were also derived from the numerical analysis and new model and from existing two-dimensional analytical models developed by Tate [3] and Rosenberg *et al.* [8]. As the other need many simulations in each velocity to obtain the critical ricochet angles, and also any change in geometry can lead to a new simulation, then this process is time-consuming subsequently, presenting a new analytical formulation might be of great importance to find the critical ricochet angle.

In order to calculate the critical ricochet angle it has been only two analytical model (Tate and Rosenberg models). As these two models usually overestimate the results comparing with test experimental setup; however, the others compare their results with these two analytical methods. As the presented method predicts the results more accurately and the errors are reduced into 25%. Then it can be a new analytical model to reach the better agreements. Therefore new analytical model can be used as a useful method to predict critical ricochet angle in metal cases.

When the target hardness was considered the numerical results predicted that a higher ricochet angle can be obtained by employing harder target materials for a given impact velocity, which was appreciable at lower velocities in particular.

NOMENCLATURE

- β Critical ricochet angle
- ρ_T Target's density
- ρ_P Projectile's density
- V Striking velocity of the rod
- L Projectile length
- D Projectile diameter
- U,u Projectile penetration velocity
- Y_P Projectile resistance
- R_T Target resistance
- S Length of the eroding tip of the projectile
- ψ Rotations of the projectile eroding surface relative to the un-deformed projectile edge
- x Projection of S in vertical direction (S.Cosψ)
- t Time
- f The force acts on the projectile
- m, m_1, m_2 Residual mass off the projectile, Projectile tip mass, Projectile eroded mass
- V_T Vertical velocity
- $\dot{l}$ Projectile erosion rate
- ν Tail velocity (Instantaneous velocity of [illegible] deformed portion of the projectile)
- α Coefficient ($\alpha = -\frac{\dot{l}}{v}$)
- λ Coefficient ($\lambda = \sqrt{\left(\frac{\rho_t}{\rho \ldots}\right)}$ [illegible]
- γ Coefficient (γ [illegible]
- Y_T target [illegible]
- σ, σ_0 Stat[illegible]
- ε_P, ε, ε_0 [illegible] rate, ref[illegible]
- B, C, n, m Mate[illegible] Cook relation
- T, T_r, T_m Tempera[illegible]perature, melting temperatu[illegible]

REFE[illegible]ENCES

1. Goldsmith, W., *Non-Ideal Projectile Impact on Targets, Chapter 10: Ricochet, Int. J. Impact Eng.*, 22, pp. 95–395 (1999).
2. Jonas, G. H. and Zukas, J. A., "Mechanics of Penetration: Analysis and Experiment," *Int. J. Eng Sci.*, 16, pp. 879–903 (1978).
3. Tate, A., "A Simple Estimate of the Minimum Target Obliquity Required for the Ricochet of a High Speed Long Rod Projectile," *J. Phys. D*, 12, pp. 1825–1829 (1979).
4. Senf, Rothenhaeusler, H. H., Scharpf, F., Poth, A. and Pfang, W., "Experimental and Numerical Investigation of the Ricocheting of Projectiles from Metallic Surfaces," *Proc. 6th Int. Symp. Ballistics*, Orlando, FL (1981).
5. Reid, S. R., Edmunds, A. J. and Johnson, W., "Bending of Long Steel and Aluminum Rods During End Impact with a Rigid Target," *J. Mech. Eng. Sci.*, 23, pp. 85–92 (1981).
6. Johnson, W, Sengupta, A. K. and Ghosh, S. K., "Plasticine Modeled High Velocity Oblique Impact and Ricochet of Long Rods," *Int. J. Mech. Sci.*, 24, pp. 437–455 (1982).
7. Johnson, W, Reid, S. R., Sengupta, A. K. and Ghosh, S. K., "Modeling with Plasticine the Low Speed Impact of Long Rods Against Inclined Rigid Targets," *Int. J. Impact Eng.*, 1, pp. 73–83 (1983).
8. Rosenberg, Z., Yeshurun, Y. and Mayseless, M., "On the Ricochet of Long Rod Projectiles," *Proc. 11th Int. Symp. Ballistics*, Brussels, Belgium (1989).
9. Orphal, D. L. and Anderson, Jr. C. E., "Test Damage from Highly Oblique Impacts of Steel Spheres Against Thin Laminated Ta[illegible]," *Int. J. Impact Eng.*, 26, pp. 567–578 (2001).
10. Roisman, I. [illegible]d Rubin, M. B., "Oblique Penetratio[illegible] Into an Elastic-Plastic Target[illegible] 769–795 (1997).
11. Zu[illegible]chet of Deforming [illegible] *J. Impact Eng.*, [illegible]
12. [illegible]xperimental Study [illegible] Hard-Core Projectile [illegible] *Int. J. Impact Eng.*, 19, [illegible]
13. [illegible]haracterizing Secondary Debris [illegible] *J. Impact Eng.*, 26, pp. 713–724 [illegible]
14. [illegible], Grote, R. and Polesne, J., "Improving [illegible]enetration Algorithm for Tomorrow's Ar[illegible] US Army Research Laboratory Report [illegible]-RP-23, Aberdeen Proving Ground, Maryland (2001).
15. Segletes, S. B., "An Adaptation of Walker-Anderson Model Elements Into the Frank-Zook Penetration Model for Use in MUVES," US Army Research Laboratory Report ARL-TR-2336, Aberdeen Proving Ground, Maryland (2000).
16. Woong, Lee, Heon-Joo, Lee and Hyunho, Shin, "Ricochet of a Tungsten Heavy Alloy Long-Rod Projectile from Deformable Steel Plates," *J. Phys. D: Appl. Phys.*, 35, pp. 2676–2686 (2002).
17. Johnson, G. R. and Cook, W. H., *Proc. 7th Int. Symp. Ballistics*, p. 541 (1983).
18. Vahedi, K., "Developments of an Analytical Method for Ballistic Impact of Long-Rod Penetrators," Doctoral Dissertation, Louisiana Tech. University (1991).
19. Meyers, M. A., *Dynamic Behavior of Materials*, New York, Wiley (1994).
20. Livermore Software Technology Corporation, *LsDyna User's Manual*, Version 970 (2007).
21. Anderson, C. E. and Walker, J. D., "An Examination of Long-Rod Penetration," *Int. J. Impact Eng.*, 11, pp. 481–501 (1991).

(Manuscript received September 7, 2007, accepted for publication February 29, 2008.)